Plasma-grating-based laser pulse compressor

G. Lehmann and K. H. Spatschek
Institut für Theoretische Physik I, Heinrich-Heine-Universität Düsseldorf, D-40225 Düsseldorf, Germany

(Received 3 April 2024; accepted 11 July 2024; published 30 July 2024)

To avoid damage in high-power laser systems, a chirped plasma-based grating is proposed for compressing laser pulses that have been previously stretched and amplified. This chirped grating is generated through the interaction of chirped pump laser pulses in a plasma slab. Particle-in-cell (PIC) simulations demonstrate that the grating exists for a duration sufficient to be utilized in the final chirped pulse amplification (CPA) stage. The generation of the grating is quite flexible, as several parameters can be adjusted, such as plasma density, chirp, length, and intensity of the pump laser. To begin, the structure of the grating is analyzed in terms of ponderomotive effects of the pump laser pulses. The primary application of the chirped plasma-based grating lies in compressing laser pulses to large amplitudes and short durations after they have been stretched and amplified beforehand. The compression factor is explored in connection with potential grating parameters. Reflectivity and effective bandwidth of chirped plasma gratings are parameters to be optimized. However, the grating spectral bandwidth can only be increased at the expense of reflectivity. The PIC results are made understandable through model calculations based on coupled mode equations.

DOI: 10.1103/PhysRevE.110.015209

I. INTRODUCTION

To avoid damage of optical components in high-power laser systems, the Nobel-Prize-worthy chirped pulse amplification (CPA) technique was developed [1,2]. Initially, pulse stretching, amplification, and compression were performed exclusively by pairs of conventional solid-state components [3]. The highest peak power is limited by the optical threshold of the compressor components. Compared to solid-state materials, plasma—being already ionized—does not suffer from breakdown at extreme light intensities. Therefore, interest of the high-intensity laser community is increasingly focused on plasma-based components to overcome the limitations posed by solid-state components [4–6]. More and more plasma-based components are becoming available for shorter laser pulse duration. The last compressor stage in a CPA chain, in particular, is of central interest [7]. Obviously, a plasma-based laser pulse compressor will promote technology. If one were to succeed in significantly increasing its efficiency, many applications in various fields would open up, aside from the breakthrough in basic research. Material processing [8], laser medicine [9,10], diagnostics of ultrafast processes in atoms and molecules [11], laser fusion [12], and so on, would definitely benefit from an increase in intensity.

A plasma-based laser pulse compressor will utilize the properties of a plasma grating. The plasma grating is a purely optically generated plasma structure that varies in time on the ion timescale. Therefore, it can be utilized for manipulating short, high-intensity laser pulses. The formation of electron and ion density gratings by the interaction of two counter-propagating laser pulses has been known for at least 20 years [13–16]. Since then, many fundamental properties have been worked out [17–30]. The plasma grating is tunable since its period can be varied when changing the angle between the pump pulses. On the other hand, a plasma does not allow one to manufacture a grating with sharp boundaries and quite homogeneous amplitude. Typically, a grating is produced by intersecting pump laser pulses. Their profiles determine the spatial envelope of the produced grating. Thereby, grating structures with constant grating periods but space-dependent envelopes appear [31,32]. A strictly homogeneous plasma grating with constant amplitude is an idealization whose limits were discussed [33]. However, understanding the differences allows us to extend many model statements obtained with constant grating amplitude to inhomogeneous gratings.

For high-power laser physics, the production of chirped plasma gratings is a major challenge for the future. One can learn a lot from the development of fiber optics [3,34–40]. Within the area of fiber optics, refractive index modification for volume chirped Bragg gratings was proposed [3] by considering the interaction of a focused laser with a defocused writing laser. It is still unknown whether this technique can be transferred to producing chirped plasma-based gratings. We shall come back to this problem in a subsequent paper. Here we prefer another idea. A chirped plasma-based grating may occur when two oppositely propagating chirped pump lasers interact within a plasma slab. There is also a third idea [41] which is based on the fact that light reflection from an inhomogeneous plasma occurs for different frequencies at different positions. We will briefly comment on this when analyzing coupled mode equations for inhomogeneous plasma. The coupled mode equations [42] demonstrate a direct analogy between a quadratically chirped and a linear inhomogeneous lattice. However, this correspondence is based on some simplifying assumptions. Therefore, it remains to be examined whether the predictions actually hold true for plasma situations. If so, it could potentially offer a simple way to realize a plasma pulse compressor.

The present work was strongly inspired by a paper by Edwards and Michel [7]. They proposed a realistic scenario

for a compact CPA system, in which the final stage comprises a homogeneous plasma transmission grating. This should compensate for low angular dispersion. Here, we raise the question of whether and how a chirped plasma grating can be produced and subsequently utilized in a CPA system. We hope that our concept could achieve compression of a chirped pulse using a single plasma-based device used in reflection, whereas Ref. [7] used a pair of transmission gratings (one of which is plasma based).

The paper is organized as follows. After the Introduction, Sec. II deals with the production of a chirped grating by two oppositely propagating laser pulses. It contains a first part where results from a PIC simulation are shown. A subsequent theoretical interpretation supports the idea that for certain configurations of the pump lasers a chirped plasma-based grating occurs. Section III is devoted to a theoretical understanding of the spectral properties of the grating. It assumes a homogeneous grating with chirp. Then, based on coupled mode equations, analytic solutions are possible. A connection to the inhomogeneous case with a Gaussian envelope would be possible by applying a discretization process, with subsequent transfer-matrix method, for nonuniform gratings [43]. However, omit this. The analytic solutions are for the Fourier components of a pulse, i.e., for a plane wave entering a chirped grating. Different frequency components of a probe pulse propagate with varying phases [36]. When a broad spectral range is separated by a grating, the latter separates different spectral components with varying phases and then recombines them. Through this combination, the original laser pulse can be restored and significantly shortened in duration. Thus, Sec. III is useful for the PIC simulations of Sec. IV where chirped pulses enter a chirped grating, and leave it compressed and unchirped. The results of Sec. IV allow for an estimate of the efficiency of a grating in reflection and the chirp compensation during compression. Appendices A and B support the theory presented in Sec. III. In Appendix A 2 we also show the analogy between chirp and inhomogeneity. A specific result is that a Gausssian envelope always produces a correction similar to quadratic chirp. The paper is concluded by a short summary and outlook.

II. BASIC CHIRPED GRATING CONFIGURATIONS

A. PIC simulations

We begin by studying the formation of density gratings via the interaction of two chirped laser pulses in underdense plasma. The plasma is assumed to be fully ionized prior to the incidence of the pump lasers. We consider counterpropagating geometry and choose x as the propagation direction. The electric fields of the pulses in vacuum, before entering plasma, are given as

$$E_{1,2}(x,t) = E_0 \exp\left[-\left(\frac{x \mp v_g t}{\tilde{\sigma}}\right)^2\right] \times \exp\{\mathrm{i}[\omega_0(1 + b_{1,2}\, t)t \mp k_0 x]\}, \quad (1)$$

where 1 belongs to the upper sign and 2 to the lower sign. Furthermore ω_0 is the central frequency, $b_{1,2}$ is the chirp parameter for linear chirp, $k_0 = 2\pi/\lambda_0$, and λ_0 is the vacuum laser wavelength. Since the pulses start in vacuum, the group velocity $v_g = \omega_0/k_0 = c$. The pulse E_1 propagates in the positive x direction, E_2 opposite to that. The coefficients $\tilde{\sigma}$ and $b_{1,2}$ can be easily given in standard form for chirped Gaussian pulses when we perform a frequency analysis at $x = 0$. The Fourier transform $E(t) = \frac{1}{\sqrt{2\pi}} \int_{-\infty}^{\infty} E(\omega) \exp(i\omega t) d\omega$ of

$$E(\omega) = \frac{\sigma}{2} \exp\left(\frac{\sigma^2(\omega - \omega_0)^2}{4}\right) \exp(-iD_2[\omega - \omega_0]^2), \quad (2)$$

with the standard coefficient D_2 for quadratic phase and Gaussian envelope width σ, is

$$E(t) = \frac{\sigma}{\sqrt{4iD_2 + \sigma^2}} \exp\left(-\frac{\sigma^2 t^2}{16D_2^2 + \sigma^4}\right) \times \exp\left(i\left[\omega_0 t + \frac{4D_2}{16D_2^2 + \sigma^4} t^2\right]\right). \quad (3)$$

This leads to

$$E_0 \mathrel{\hat{=}} A = \frac{\sigma}{\sqrt{4iD_2 + \sigma^2}}, \quad \frac{v_g^2}{\tilde{\sigma}^2} \mathrel{\hat{=}} B = \frac{\sigma^2}{16D_2^2 + \sigma^4}, \quad b \mathrel{\hat{=}} \frac{1}{\omega_0} \frac{4D_2}{16D_2^2 + \sigma^4}. \quad (4)$$

Depending on the sign of D_2 we have positive ($b > 0$) or negative ($b < 0$) chirp. The minimal pulse duration $\tau_{\min} = 2\sigma\sqrt{\ln(2)}$ is obtained for $D_2 = 0$. For finite D_2, the FWHM duration of the chirped pulse τ_{ch} is

$$\tau_{\mathrm{ch}} = \tau_{\min} \sqrt{1 + \left(\frac{16 D_2 \ln(2)}{\tau_{\min}^2}\right)^2}. \quad (5)$$

For $b_{1,2} > 0$, the pulse will be up-chirped, i.e., the instantaneous frequency ω will rise from head to tail of the pulse (irrespective of the propagation direction). The unchirped case $b_{1,2} = 0$ corresponds to the bandwidth limited pulse, the shortest laser pulse possible given the bandwidth of the laser. In what follows, we will always assume that the bandwidth of the laser pulses is constant, i.e., the pulses $E_{1,2}$ originate from the same laser. Then $|b_{1,2}| \neq 0$ will always lead to pulses longer than the bandwidth limited FWHM duration $\tau_{\min}$. The sign of $b_{1,2}$ determines up- or down-chirp, but has no influence on pulse duration.

Let us now assume, without loss of generality, that both pulses have the same amount $|b_{1,2}|$ of chirp. We can then distinguish between two cases. In the first case, both pulses are either up- or down-chirped. In the second case, one of the pulses is up-chirped, the other one is down-chirped. As we shall discuss later, this second case is equivalent to the situation where one pulse is unchirped (i.e., bandwidth limited) and the second pulse is chirped at a rate twice as large.

In order to study the generation of chirped density gratings we performed PIC simulations using the EPOCH code [44]. In all simulations discussed in the following, the spectral bandwidth of all laser pulses is the same and the temporal pulse shape is Gaussian. We define bandwidth as the full width at half maximum (FWHM) of the magnitude of the electric field in frequency space, i.e., of $|E(\omega)|$. The pulses only differ in their spectral phase, i.e., $\arg[E(\omega)]$ due to the parameter $b_{1,2}$. We consider a central laser wavelength of $\lambda_0 = 800$,

i.e., $\omega_0 = 2.35 \times 10^{15}$ s^{-1}, and assume that for $b_{1,2} = 0$ we have pulses with FWHM duration of 30 fs. This corresponds to a frequency bandwidth $\Delta\omega = 0.078\,\omega_0$ or a wavelength bandwidth in vacuum of approximately 800 ± 62 nm.

In all simulations, we use 20 cells per λ_0 and 250 particles per cell and per species. We simulate hydrogen plasma with mobile ions of mass $m_i = 1836\,m_e$, electron temperature $T_e = 1$ eV and ion temperature $T_i = T_e/10$. In the center of the simulation box we have an $800\,\lambda_0$ long plasma slab of initially homogeneous density $n_0 = 0.05\,n_c$, where $n_c = \omega_0^2 \epsilon_0 m_e / e^2$. To the left and right of the plasma there is sufficient vacuum, $2500\,\lambda_0$ on each side, to fully cover all incoming and outgoing laser fields. The position $x = 0$ is in the center of the plasma, where the maxima of the two pulses overlap at $t = 0$.

1. The case $b = b_1, b_2 = 0$

We begin by discussing the case where only the laser field E_1 is chirped, i.e., stretched to a longer duration. The second laser pulse E_2 is assumed to be bandwidth limited, i.e., of 30 fs FWHM duration ($b_2 = 0$). The pulse E_+ is chirped such that it is 100 times longer than the short pulse ($b_1 = 1.31 \times 10^{10}$ s^{-1}, i.e., $D_2 = 8.1 \times 10^{-27}$ s^2). Both pulses have the same peak intensity of 2.5×10^{14} W/cm^2, implying that the long pulse carries 100 times the energy of the short pulse. The length of the total interaction region between the two pulses is mainly determined by the length of the long pulse and is about $600\,\lambda_0$ long. The beat electric field of the two overlapping laser pulses will initiate the formation of an electron density grating. Wavelength and frequency of the beat field will be spatially varying due to the chirp of the long pulse.

Figure 1(a) shows the electron density 12.6 ps after the interaction. In the interaction region, the plasma density is modulated by fast oscillations with wave numbers $k = 2k_1$, where $k_1 = k_0\sqrt{1 - n_0/n_c}$. Due to the temporal Gaussian envelopes of the two laser pulses, the envelope of the density modulation is also Gaussian [33]. Ion and electron densities are almost the same. Figure 1(b) shows a spectrogram of the density modulation, making the changes in the local wave number visible. The interaction between the two pulses E_1 and E_2 begins at $x = 400\,\lambda_0$, where the low-frequency components of E_1 beat with the unchirped pulse E_2. Towards the end of the interaction, E_2 propagated to $x = -400\,\lambda_0$, beating with the high-frequency components of E_1. The result is a linearly chirped plasma density grating.

2. The case $b_1 = b_2 = b$

When $b_1 = b_2 = b$, both laser pulses E_1 and E_2 have the same chirp. Both pulses are now either up- or down-chirped, depending on the sign of b. Independent of the precise value of b, the resulting plasma density grating is not chirped, and, as we shall discuss in Sec. II B, the length of the grating as well as the modulation period is practically equivalent to that resulting from the interaction of two unchirped pulses of same bandwidth.

Figure 2 shows the plasma density grating resulting from the interaction of two up-chirped pulses with $b = 1.3 \times 10^{11}$ s^{-1} (i.e., $D_2 = 8.1 \times 10^{-28}$ s^2) of intensity 2.5×10^{14} W/cm^2. This chirp rate corresponds to a tenfold temporal stretching of the original 30 fs pulse. For comparison

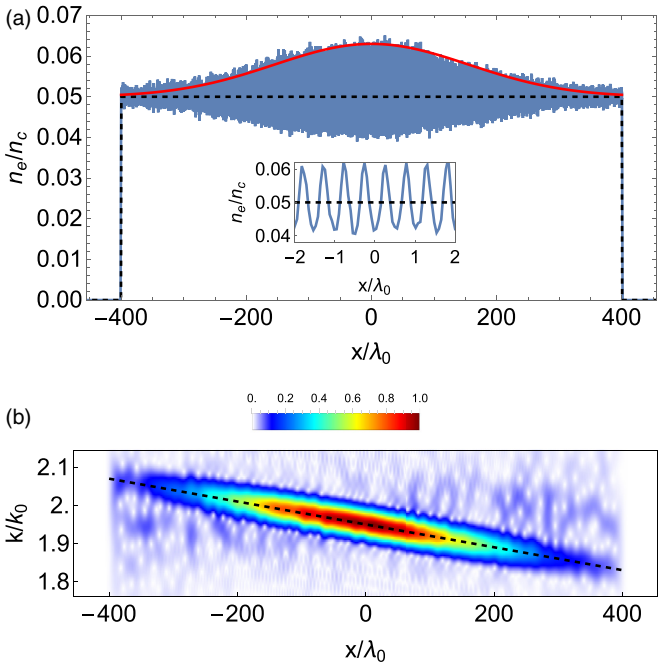

FIG. 1. (a) Electron density (blue) n_e at $t = 12.6$ ps, fast oscillations on scale of $\lambda_0/2$ can be seen in the inset. The envelope of the density variation is shown as red solid line, the initial density profile is shown as black dashed line. (b) Normalized spectrogram of the electron density variation $\delta n_e = n_e - n_0$ for n_e shown in (a), depicting which wave number contributes to the density oscillation at which position in the plasma grating. Shown are the respective Fourier amplitudes on a linear scale. The black dashed line shows the analytic result discussed at the end of Sec. II B 3.

Fig. 2 additionally shows the density grating driven by to two unchirped 30 fs pulses with intensities of 2.5×10^{15} W/cm^2. The two gratings in Fig. 2 are identical. This seemingly unspectacular result has important practical consequences for the production of plasma gratings in experiments. It shows that residual chirp on the driving pulses $E_{1,2}$ does not harm

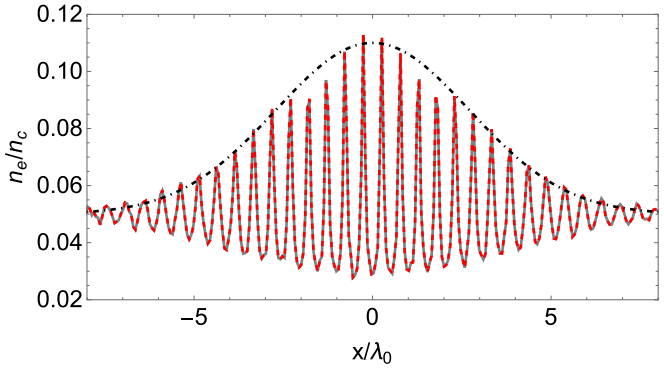

FIG. 2. Electron density n_e at $t = 4.7$ ps resulting from the interaction of two up-chirped laser pulses of 300 fs duration with intensity 2.5×10^{14} W/cm^2 (solid gray line). The density modulation resulting from the interaction of two unchirped 30 fs long pulses with intensity 2.5×10^{15} W/cm^2 is shown as a red dashed line. The black dash-dotted line shows the envelope of the density modulation as obtained from the analytic estimate (20).

the production of gratings, as long as both pulses have the same chirp profile.

B. Basic understanding of the grating structures observed in PIC simulations

In this interpretative section, we describe the chirped laser pulse as

$$E(\tau) = Ae^{-B\tau^2} e^{i\omega_0(\tilde{\tau}+b\tilde{\tau}^2)}. \tag{6}$$

We distinguish between phase propagation with phase velocity $\frac{\omega_0}{k_0}$ (described by the retarded time $\tilde{\tau}$) and envelope propagation with group velocity v_g (described by the retarded time τ). When assuming $n_0 \ll n_c$, then $\omega_0 \approx ck_0$ applies. In that case, a distinction between τ and $\tilde{\tau}$ is no longer necessary, and the representation would be somewhat simplified.

Pulse 1 should propagate from left to right and has retarded times

$$\tau \to \tau_1 = \bar{t} - \frac{1}{v_g}(x + x_0), \quad \tilde{\tau} \to \tilde{\tau}_1 = \bar{t} - \frac{k_0}{\omega_0}(x + x_0), \tag{7}$$

when starting at time $\bar{t} = 0$ at $x = -x_0 < 0$. We reserve the determination of the time origin and therefore denote the time as $\bar{t}$. On the other hand, pulse 2 should propagate from right to left and has retarded times

$$\tau \to \tau_2 = \bar{t} + \frac{1}{v_g}(x - x_0), \quad \tilde{\tau} \to \tilde{\tau}_2 = \bar{t} + \frac{k_0}{\omega_0}(x - x_0), \tag{8}$$

when starting at time $\bar{t} = 0$ at $x = x_0$.

The ponderomotive potential will be proportional to the product $E_1 E_2^* + \text{c.c.}$ We first calculate the contribution from the envelopes, starting with the cases $B_1 = B_2 \equiv B$:

$$S_1 := e^{-B\tau_1^2} e^{-B\tau_2^2} = \exp\left[-\frac{\sigma^2}{16D_2^2 + \sigma^4}\left(\frac{2}{v_g^2}x^2 + 2t^2\right)\right] \tag{9}$$

with $t = \bar{t} - \frac{1}{v_g}x_0$. On the other hand, for $b_2 = 0$ and $b_1 \equiv b$, we obtain

$$S_1 := e^{-B\tau_1^2} e^{-\sigma^{-2}\tau_2^2} = \exp\left[-\frac{16D_2^2 + 2\sigma^4}{\left(16D_2^2 + \sigma^4\right)\sigma^2}\left(\frac{1}{v_g^2}x^2 + t^2\right)\right] \times \exp\left[\frac{-16D_2^2}{\left(16D_2^2 + \sigma^4\right)\sigma^2}\frac{2}{v_g}x\,t\right]. \tag{10}$$

Now, $t = 0$ corresponds to maximum overlap of the two pump pulses.

Next, we evaluate the product of the phase factors

$$S_2 := e^{i\omega_0(\tilde{\tau}_1 + b_1\tilde{\tau}_1^2)} e^{-i\omega_0(\tilde{\tau}_2 + b_2\tilde{\tau}_x^2)}. \tag{11}$$

A short calculation leads to

$$S_2 = \begin{cases} \exp\{-2ik_0x[1 + 2b(t + t_\varepsilon)]\} & \text{for } b = b_1 = +b_2, \\ \exp\left\{-2ik_0x\left(1 - \frac{k_0}{\omega_0}bx\right)\right\} e^{2ib\omega_0(t+t_\varepsilon)^2} & \text{for } b = b_1 = -b_2, \\ \exp\left\{-2ik_0x\left[1 - \frac{k_0}{\omega_0}\frac{b}{2}x + b(t + t_\varepsilon)\right]\right\} e^{ib\omega_0(t+t_\varepsilon)^2} & \text{for } b = b_1,\ b_2 = 0, \end{cases} \tag{12}$$

where

$$t_\varepsilon = \left(\frac{1}{v_g} - \frac{k_0}{\omega_0}\right)x_0 \approx 0. \tag{13}$$

In most cases, the limit $16D_2^2 \gg \sigma^4$ will be of special interest since that limit covers the situation with significant chirp.

1. The case $b = b_1 = -b_2 \neq 0$

The forecast for that case of interacting chirped pump lasers of opposite chirp is straightforward. A spatially chirped grating with linear chirp should appear. The grating should have a spatial density variation

$$\frac{\delta n}{n_0} \sim a(x)\cos\left[2k_0x\left(1 - \frac{k_0}{\omega_0}bx\right)\right]. \tag{14}$$

Its Gaussian-type envelope $a(x)$ should be proportional to

$$a(x) \sim \exp\left(-\frac{2}{v_g^2}\frac{\sigma^2}{16D_2^2 + \sigma^4}x^2\right) \approx \exp\left(-\frac{1}{v_g^2}\frac{\sigma^2}{8D_2^2}x^2\right). \tag{15}$$

The chirp factor increases the width.

Summarizing, a chirped grating appears with varying wave number $K = 2k_0 - \frac{2k_0^2 b}{\omega_0}x$. The grating is of Gaussian form with a width (FWHM), e.g., for $16D_2^2 \gg \sigma^4$,

$$W = \sqrt{2\ln 2}\, v_g \frac{\sqrt{16D_2^2 + \sigma^4}}{\sigma} \approx 4\sqrt{2\ln 2}\, v_g \frac{|D_2|}{\sigma}. \tag{16}$$

Its width increases with chirp of the pumps.

2. The case $b = b_1 = +b_2 \neq 0$

In this case, a grating with fixed lattice spacing

$$\frac{\delta n}{n_0} \sim a(x)\cos[2k_0x] \tag{17}$$

appears. For its envelope distribution two factors arising from (9) and (12) are relevant, namely

$$\exp\left[-\frac{2\sigma^2t^2}{16D_2^2 + \sigma^4}\right] \quad \text{and} \quad \exp[-4ik_0bx(t + t_\varepsilon)]. \tag{18}$$

Let us consider the integral

$$\int e^{-2Bt^2}\exp\left[-4ik_0b(t+t_\varepsilon)x\right]dt = \frac{1}{2\sqrt{2}}\sqrt{\frac{\pi}{B}}\exp\left\{-\frac{2k_0^2b^2x^2}{B}\right\}\mathrm{erf}\left(\sqrt{2B}t+i\frac{2k_0bx}{\sqrt{2B}}\right)\times\exp(-4ik_0bt_\varepsilon x). \tag{19}$$

The overlapping of pulses occurs during a short time compared with the total existence time of the grating. Therefore, we average over time such that for $t_\varepsilon \approx 0$ the x dependence $\exp\{-\frac{2k_0^2b^2x^2}{B}\}$ survives together with a constant factor. We combine with $\exp(-\frac{\sigma^2}{16D_2^2+\sigma^4}\frac{2}{v_g^2}x^2)$ from (9) to obtain the product

$$\exp\left(-\frac{2k_0^2b^2x^2}{B}\right)\exp\left(-\frac{\sigma^2}{16D_2^2+\sigma^4}\frac{2}{v_g^2}x^2\right) = \exp\left(-\frac{2x^2}{\sigma^2}\frac{1}{v_g^2}\right)e^{-\varepsilon x^2} \tag{20}$$

with

$$\varepsilon = \frac{2}{\sigma^2}\frac{16D_2^2}{16D_2^2+\sigma^4}\left(\frac{k_0^2}{\omega_0^2}-\frac{1}{v_g^2}\right)\approx 0 \quad \text{for } n_0 \ll n_c. \tag{21}$$

Summarizing, no chirp appears in the grating. The grating is of Gaussian form with a width (FWHM)

$$W = \sqrt{2\ln 2}\, v_g\sigma \tag{22}$$

for $t_\varepsilon \sim \varepsilon \approx 0$. Its width does not depend on the chirp of the pumps.

3. The case $b_1 = b$, $b_2 = 0$

This encompasses both effects encountered in preceding subsections, namely chirp and length modification. First, a spatial density variation with chirp,

$$\frac{\delta n}{n_0} \sim a(x)\cos\left[2k_0x\left(1-\frac{k_0}{\omega_0}\frac{b}{2}x\right)\right], \tag{23}$$

occurs. Second, for the calculation of the width in x we need the integral

$$\int e^{-(A_1-iA_4)t^2-(A_2+iA_3)tx}\,dt = \frac{1}{2}\sqrt{\frac{\pi}{A_1-iA_4}}\exp\left\{\frac{(A_2+iA_3)^2x^2}{4(A_1-iA_4)}\right\}\times\mathrm{erf}\left(\sqrt{A_1-4A_4}t-\frac{A_2+iA_3}{2\sqrt{A_1-iA_4}}x\right) \tag{24}$$

with appropriate definitions of A_1, A_2, A_3, and A_4, which can be deduced from (10) and (12).

Without repeating similar calculations as before, we summarize that the envelope of the grating is of Gaussian form. For $16D_2^2 \gg \sigma^4$, its spatial width (FWHM) is

$$W = 4\sqrt{\ln 2}\, v_g\frac{|D_2|}{\sigma}. \tag{25}$$

The situation where only one pulse is chirped and the other is not corresponds to the case of two oppositely chirped pulses with half the value of b. Figure 1(b) then allows a comparison to Eq. (14). The gradient $d(k/k_0)/d(x/\lambda_0)$ can be visually estimated from Fig. 1(b) as 3×10^{-4}. Taking the spatial derivative of the phase in the cosine term in Eq. (14) results in $d(k/k_0)/d(x/\lambda_0) = 4\pi b/\omega_0 = 2.8\times10^{-4}$.

III. SPECTRAL PROPERTY OF HOMOGENEOUS GRATING WITH LINEAR CHIRP

A. Solution of coupled mode equations for single spectral components

To analyze the spectral properties of the obtained chirped grating (however, in constant envelope approximation) we start from the standard coupled mode equations (A16) and (A17) for

$$D \equiv 0, \quad C = \text{const.}, \quad \varphi(\xi) = \beta(\xi-\xi_0)^2. \tag{26}$$

We assume propagating plane waves (Fourier modes) within the slowly varying envelope approximation. The notation follows from Appendix A. Then, the basic equations are

$$\frac{du(\xi)}{d\xi} = i\left[\frac{1}{N_0^2}\Delta-\beta(\xi-\xi_0)\right]u(\xi)+iC_0\,v(\xi), \tag{27}$$

$$\frac{dv(\xi)}{d\xi} = -i\left[\frac{1}{N_0^2}\Delta-\beta(\xi-\xi_0)\right]v(\xi)-iC_0\,u(\xi), \tag{28}$$

where β and $C_0 = \frac{1}{4}(1-\frac{1}{N_0^2})C < 0$ are constants. The variable u corresponds to the envelope of the incoming (and transmitted) wave while v describes the reflected wave. As before, the frequency mismatch Δ is a fixed parameter. In that case, analytic solutions are possible.

Let us rewrite Eqs. (27) and (28) with

$$Z(\xi) = \frac{1}{N_0^2}\Delta\xi-\frac{1}{2}\varphi(\xi), \quad Z'(\xi) = \frac{1}{N_0^2}\Delta-\beta(\xi-\xi_0), \quad Z''(\xi) = -\beta, \tag{29}$$

and introduce

$$\bar{u} = ue^{-iZ}, \quad \bar{v} = ve^{iZ}. \tag{30}$$

Then we obtain

$$\frac{d^2\bar{u}(\xi)}{d\xi^2}+2iZ'\frac{d\bar{u}(\xi)}{d\xi}-C_0^2\bar{u} = 0, \tag{31}$$

$$\frac{d^2\bar{v}(\xi)}{d\xi^2}-2iZ'\frac{d\bar{v}(\xi)}{d\xi}-C_0^2\bar{v} = 0. \tag{32}$$

We may transform this set of equations into standard forms for known polynomials by defining the dimensionless space variable

$$\zeta = C_0(\xi-\xi_0)-\frac{C_0}{\beta N_0^2}\Delta \;\rightsquigarrow\; \xi = \frac{\zeta}{C_0}+\frac{\Delta}{N_0^2\beta}+\xi_0, \tag{33}$$

and changing the dependent variables into

$$U(\zeta) \equiv \bar{u}(\xi), \quad V(\zeta) \equiv \bar{v}(\xi). \tag{34}$$

Note that

$$V(\zeta) = -i\frac{dU(\zeta)}{d\zeta}\, e^{2iZ}, \tag{35}$$

$$U(\zeta) = -i\frac{dV(\zeta)}{d\zeta}\, e^{-2iZ} \tag{36}$$

holds. The set of equations

$$\frac{d^2U}{d\zeta^2} = i\chi_1\zeta\frac{dU}{d\zeta} + U, \tag{37}$$

$$\frac{d^2V}{d\zeta^2} = -i\chi_1\zeta\frac{dV}{d\zeta} + V \tag{38}$$

with

$$\chi_1 = \frac{2\beta}{C_0^2} \tag{39}$$

will appear. The system of differential equations can be solved in various ways.

Here, in the main text, we present a solution with Kummer functions. Alternatively, one may use Hermite polynomials as shown in Appendix B.

Starting from Eqs. (37) and (38), we now introduce the new coordinate

$$z = \frac{i}{2}\chi_1\zeta^2. \tag{40}$$

Then the coupled mode equations become

$$z\frac{d^2U}{dz^2} + \left(\frac{1}{2} - z\right)\frac{dU}{dz} + i\frac{1}{2\chi_1}U = 0, \tag{41}$$

$$z\frac{d^2V}{dz^2} + \left(\frac{1}{2} + z\right)\frac{dV}{dz} + i\frac{1}{2\chi_1}V = 0. \tag{42}$$

For the first equation, two independent solutions can be written in terms of confluent hypergeometric functions of the first kind, also known as Kummer functions $M(a, b, z)$ as (see also Ref. [36])

$$U_1(\zeta) = M\left(-i\frac{1}{2\chi_1}, \frac{1}{2}, \frac{i}{2}\chi_1\zeta^2\right), \tag{43}$$

$$U_2(\zeta) = \zeta\, M\left(\frac{1}{2} - i\frac{1}{2\chi_1}, \frac{3}{2}, \frac{i}{2}\chi_1\zeta^2\right). \tag{44}$$

Similarly for the second equation

$$V_1(\zeta) = M\left(i\frac{1}{2\chi_1}, \frac{1}{2}, -\frac{i}{2}\chi_1\zeta^2\right), \tag{45}$$

$$V_2(\zeta) = \zeta\, M\left(\frac{1}{2} + i\frac{1}{2\chi_1}, \frac{3}{2}, -\frac{i}{2}\chi_1\zeta^2\right). \tag{46}$$

From here we define the general solutions with so far arbitrary coefficients A_1, A_2, B_1, and B_2, i.e.,

$$U(\zeta) = A_1\, U_1(\zeta) + A_2\, U_2(\zeta), \tag{47}$$

$$V(\zeta) = B_1\, V_1(\zeta) + B_2\, V_2(\zeta). \tag{48}$$

In addition, we use (35) and (36) with

$$Z = \frac{\Delta}{N_0^2}\left[\frac{1}{2}\frac{\Delta}{N_0^2\beta} + \xi_0\right] - \frac{\beta}{2C_0^2}\zeta^2. \tag{49}$$

The boundary condition $V(\zeta_+) = 0$ leads to

$$\rho \equiv \frac{B_2}{B_1} = -\frac{M\left(i\frac{1}{2\chi_1}, \frac{1}{2}, -\frac{i}{2}\chi_1\zeta_+^2\right)}{M\left(\frac{1}{2} + i\frac{1}{2\chi_1}, \frac{3}{2}, -\frac{i}{2}\chi_1\zeta_+^2\right)}, \tag{50}$$

where $\xi_0 = 2\pi N_0 x_0$. For further relations we do not use a normalized input at $\zeta = \zeta_-$. Instead, we compare the series expansion of $U(\zeta)$ with that of $V(\zeta)$ making use of (35) and (36). A short calculation leads to

$$\frac{A_1}{B_2} = ie^{-i\theta}, \quad \frac{B_1}{A_2} = -ie^{i\theta}, \quad \theta = 2\frac{\Delta}{N_0^2}\left[\frac{1}{2}\frac{\Delta}{N_0^2\beta} + \xi_0\right],$$
$$\rho = \frac{B_2}{B_1} = \frac{A_1}{A_2}. \tag{51}$$

For calculating reflection and transmission, respectively, the two quantities

$$r = \frac{\tilde{v}(\xi_-)}{\tilde{u}(\xi_-)} = \exp\left[-4\pi i N_0\Delta + i\frac{\Delta^2}{N_0^4\beta} - i\frac{\pi}{2}\right] \times \frac{V_1(\zeta_-) + \rho V_2(\zeta_-)}{\rho U_1(\zeta_-) + U_2(\zeta_-)}, \tag{52}$$

$$t = \frac{\tilde{u}(\xi_+)}{\tilde{u}(\xi_-)} = \exp\left[-4\pi i N_0\Delta\left(1 - \frac{1}{N_0^2}\right)L\right] \times \frac{\rho U_1(\zeta_+) + U_2(\zeta_+)}{\rho U_1(\zeta_-) + U_2(\zeta_-)} \tag{53}$$

are obtained with the help of (51). Then, the reflection coefficient R and the transmission coefficient T follow from

$$R = |r|^2 = \left|\frac{V_1(\zeta_-) + \rho\, V_2(\zeta_-)}{\rho\, U_1(\zeta_-) + U_2(\zeta_-)}\right|^2 \tag{54}$$

and

$$T = |t|^2 = \left|\frac{\rho\, U_1(\zeta_+) + U_2(\zeta_+)}{\rho\, U_1(\zeta_-) + U_2(\zeta_-)}\right|^2. \tag{55}$$

These formulas lead to results that are identical to (B11) and (B12), respectively.

Note that in (A5) the normalized frequency mismatch Δ is defined with respect to ω_0. However, when we choose $x_0 = -L$, the resonance frequency ω_0 occurs at the entrance of the grating, i.e., at $x = -L$. Very often, the frequency deviation is defined with respect to the resonance frequency in the middle of the grating, i.e., at $x = 0$. In that case, we shift Δ by $2\pi N_0|\beta|L$. This shift becomes obvious from (A9) and (A10). We may write in nondimensional form

$$\psi = 4\pi N_0 x + 4\pi^2 N_0^2\beta(x - x_0)^2, \tag{56}$$

leading via $k_{\rm eff} = \partial\Psi/\partial x$ to

$$k_{\rm eff} = 4\pi N_0[1 + 2\pi N_0\beta(x - x_0)] \tag{57}$$

for the effective wave number of the grating. Therefore, we introduce

$$\tilde{\Delta} = \Delta + 2\pi N_0|\beta|L \tag{58}$$

for the following plots when the resonance frequency occurs in the middle of the grating.

B. Forecasts for parameter dependencies

Next we discuss the properties of a more realistic chirped plasma-based grating. We pose the question of effectiveness by varying different parameters. The grating (for $b_1 = b$ and $b_2 = 0$) may be written in the form

$$\delta n_e = C \cos\left[4\pi N_0 x + 4\pi^2 N_0^2 \beta (x - x_0)^2\right], \qquad (59)$$

where the density perturbation δn_e is normalized by n_0 and x is normalized by λ_0. For the theoretical forecast, the grating is assumed to be spatially homogeneous, existing in the region $-L \leqslant x \leqslant L$.

We start now from the parameter set

$$L \equiv L_0 = 270, \quad \beta \equiv \beta_0 = -2.35 \times 10^{-5}, \quad C \equiv C_0 = 0.2, \qquad (60)$$

and $n_0 = 0.05 n_c$. The initial position is $x_0 = -L$, where the grating starts with wave number $2k_0$. As before, shifting the resonance to the center of the grating is done afterwards by changing Δ to $\tilde{\Delta}$. The sign of the grating chirp is such that the probe pulse arrives on the side of the grating where the large wave numbers are.

1. *Reflection in dependence of various parameters*

We use (54) and (55) to study how variations of these parameters affect reflection and transmission. For clarity of presentation, we will only discuss reflection as transmission follows via $T = 1 - R$. Even though in a realistic setting grating amplitude, length, and chirp will depend on each other, we shall treat them as independent for this section in order to see the influence of each parameter separately.

Let us start with a variation of the chirp parameter β; results are shown in Fig. 3(a). We observe a clear dependence on the strength of the chirp parameter for both the bandwidth and the strength of the reflection behavior. Within the reflection windows, different frequencies are reflected with almost the same amplitudes. The observed oscillations in the reflection coefficient are similar to earlier predictions for Bragg gratings with linear chirp [36,40]. Obviously, chirp increases the window width (bandwidth) while decreasing the reflectivity.

Next, we vary the strength of the grating, i.e., the parameter C. Results are shown in Fig. 3(b). Increasing the grating amplitude obviously does not alter the bandwidth in Δ for the reflection. However, it does lead to the expected increase in the reflection rate.

Finally, we vary the total length $2L$ of the grating. Results are shown in Fig. 3(c). Varying the length of the grating results in a change in the reflection window. Longer lattices allow for a larger bandwidth in Δ. However, the length does not significantly influence the strength of the reflection.

2. *Bragg reflection points*

Different frequency contributions are effectively reflected at different depths in the grating. A typical example is depicted in Fig. 4.

Two understand this phenomenon, we briefly refer to the standard theory of Bragg reflection. A first estimate can be obtained along the following line. Recognizing relatively small windows for reflection in the chirpless case $\beta = 0$, we introduce a coarse grained detuning parameter $\bar{\Delta}$ which corresponds to the center of the chirpless reflection window.

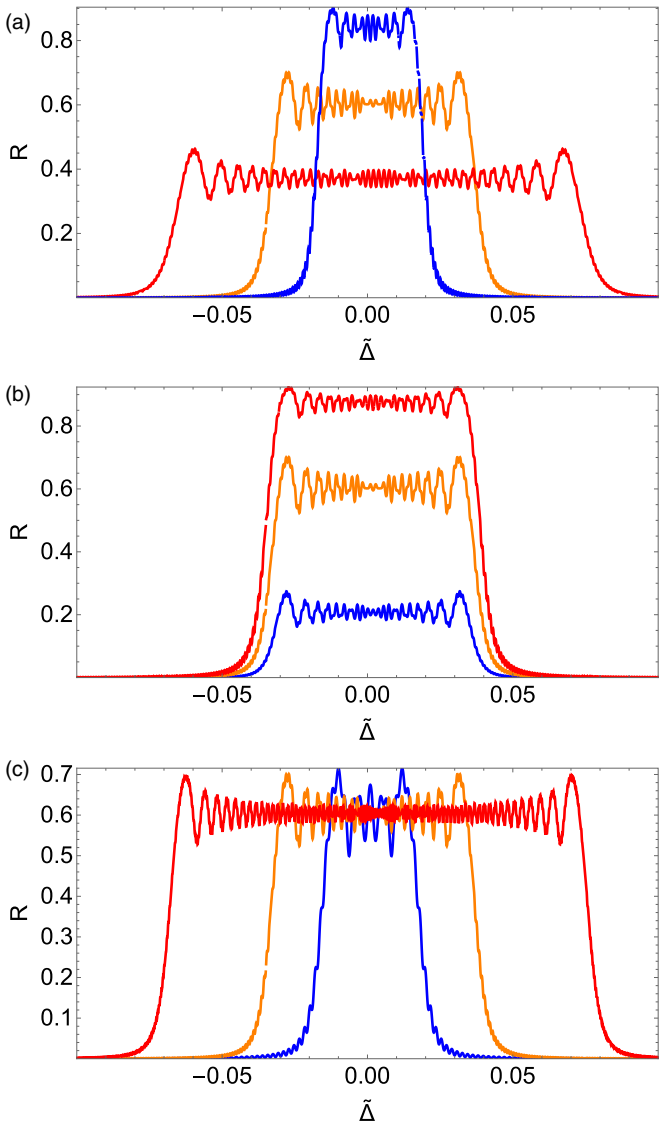

FIG. 3. (a) Kummer function solutions of (37) and (38) for chirp rates $\beta_0/2$ (blue line), β_0 (orange line), and $2\beta_0$ (red line). Grating amplitude $C = 0.2$ and length $L = 270$ are fixed. (b) Results for fixed chirp rate β_0 and fixed grating length L_0, but amplitudes $C = 0.1$ (blue line), $C = 0.2$ (orange line), and $C = 0.3$ (red line), respectively. (c) Results for variation of the grating length $L = L_0/2$ (blue line), $L = L_0$ (orange line), and $L = 2L_0$, respectively. Grating amplitude $C = 0.2$ and chirp rate β_0 are fixed. Shown in all panels is the reflection coefficient R in dependence of frequency mismatch $\Delta = \tilde{\Delta}$.

We have $\bar{\Delta} = 0$ for $\beta = 0$. Then, using (57) we estimate the points of reflection x_B from

$$\bar{\Delta} \approx 2\pi N_0 \beta (x_B - x_0). \qquad (61)$$

For $x_0 = -L$

$$x_B = \frac{\bar{\Delta}}{2\pi N_0 \beta} - L \qquad (62)$$

follows. When analyzing the distributions in Fig. 4, we find excellent agreement with the analytic prediction. Note that $\Delta = -0.01$ might be interpreted as $\bar{\Delta} \approx 0$ and $\Delta = -0.08$ as $\bar{\Delta} \approx -0.08 \pm 0.01$.

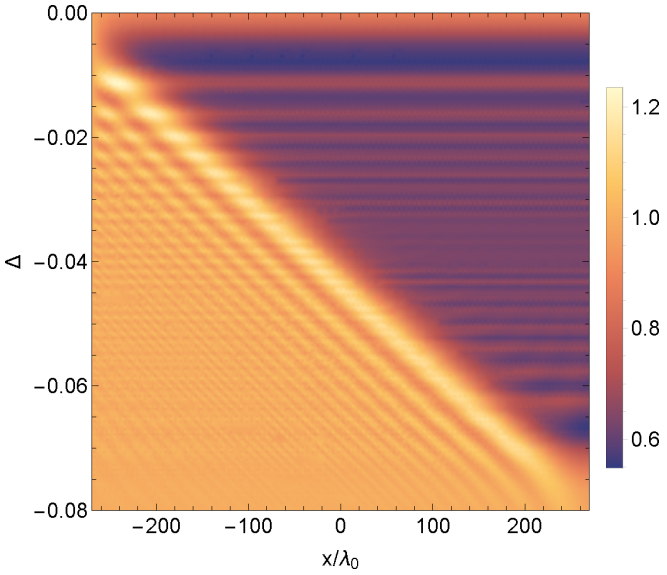

FIG. 4. Absolute value of the transmitted wave amplitude as a function of x for different frequencies Δ as obtained from Hermite function solutions (B6). Parameters are (60). Clearly, for the different frequencies, the points of effective reflection are different.

The more precise method, almost used as standard [36], calculates the group delay starting from (52),

$$f = \frac{d\,\arg(r)}{d\,\Delta} = \frac{d\ \mathrm{Im}\ln(r)}{d\,\Delta}. \tag{63}$$

Various contributions can be identified. Around a mean slope, there are ripples, also called chirped oscillations. Additional oscillations occur at the border of significant reflection In our case, the mean slope can be identified form the first (exponential) factor on the right-hand side (r.h.s.) of (52). It shows the same behavior $\sim\frac{\Delta}{\beta}$ as estimated in (62). The r.h.s. of (52), at least concerning the first factor, also explains the result already shown in Fig. 3(c), namely that the strength of the reflection does not depend on the length L.

IV. PULSE COMPRESSION BY A CHIRPED PLASMA GRATING

Chirped plasma density gratings could provide the means to compress chirped high-power laser pulses in reflection, very similar to conventional solid-state gratings in CPA schemes. Solid-state gratings usually have to be operated at fluences below 0.1 J/cm^2 for 30 fs pulses, translating to peak intensities of about 10^{12} W/cm^2. Such intensities are close to the ionization threshold of solid-state material, which is why the compressor gratings have to be adequately sized (several hundreds of cm^2 for petawatt systems). Repetition rates of CPA-based laser systems at the same time are currently limited to about 1 Hz (PW level lasers) to 10 Hz (0.1 PW level lasers). Higher rates are desirable to increase the average power which in turn increases average power of, e.g., laser driven radiation or particle sources. Current limitations in repetition rate are mainly due to pumping processes of the laser, cooling of the amplifiers, but also due to heat induced deformation of the compressor gratings [45–47].

Plasma compressor gratings could provide remedy for two issues. Their damage threshold is usually determined by the fact that the density modulation should not be altered by the ponderomotive potential of the probe pulse. This translates for typical underdense plasmas to intensities close to 10^{17} W/cm^2, i.e., five orders of magnitude higher than for solid-state gratings. At the same time, one could use a fresh plasma grating for every shot, which could allow for repetition rates far beyond a few Hz.

A. PIC results

To demonstrate that pulse compression is possible, we study the reflective properties of the grating previously discussed in Sec. II. Once the grating is fully established, we continue the simulation and send a chirped laser pulse onto the grating. The chirp rate of this probe pulse is the same as that of the chirped driver pulse. If the compression was perfect, we would expect the reflected pulse to have a 100 times shorter duration and at the same time a 100 times higher intensity. For demonstration purposes we use a probe intensity of 10^{14} W/cm^2. Figure 5 shows the electric field of the incoming probe (moving from left to right) and that of the reflected part of the probe. The fields in Fig. 5(a) are normalized to the maximum of the incoming pulse. The reflected pulse is clearly very much shorter than the incoming pulse, but the maximum electric field is only about 5 times larger than that of the incoming pulse. The intensity of the reflected pulse is about 27 times larger. The main reason for not achieving an intensity increase by a factor of 100 is that about 50% of the incoming laser energy is transmitted by the grating. In particular energies of frequencies in the wings of the probe spectrum are not sufficiently reflected. This decreases the de facto bandwidth of the laser pulse. Accordingly, we measure a FWHM duration of the reflected pulse of about 50 fs. The spectrum of the reflected pulse has almost a flat phase, i.e., little residual chirp, which is mostly quadratic chirp, originating from the spatial inhomogeneity of the grating amplitude. Overall, the grating reflects 50% of the pulse energy and produces spectral narrowing, leading to an increase in pulse duration. An increase in plasma temperature from $T_e = 1$ eV to $T_e = 10$ eV results in about 10% less total reflected energy.

The coupled mode equations show that reflectivity and effective bandwidth of chirped plasma gratings are parameters to be optimized. The grating spectral bandwidth can be increased at the cost of reflection efficiency. We shall leave this optimization process for a future work, addressing in more detail a realistic implementation of a holographic CPA compressor grating.

B. Comparison of PIC results with model predictions

Let us use parameters approximating the situation discussed in Sec. II. We choose the values (60). The initial position is $x_0 = -L$, where the grating starts with wave number $2k_0$. The sign of the grating chirp is such that the probe arrives at the side of the grating where the large wave numbers are.

Figure 6 shows the result for the reflection coefficient obtained from (54) and compared to the corresponding spectral data of the PIC simulation. From the PIC data shown in Fig. 5(b) R is obtained by normalizing per frequency the absolute reflectivity to the incoming spectral amplitude. We

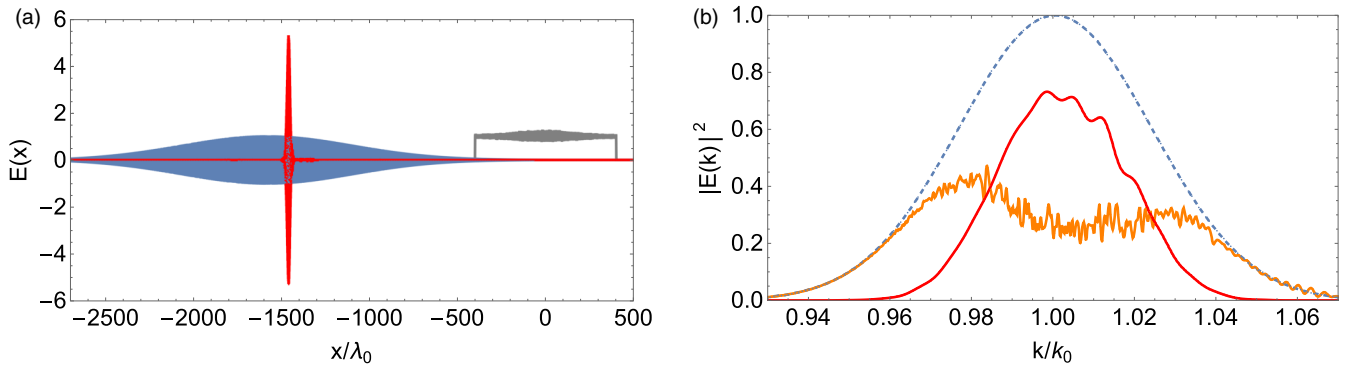

FIG. 5. (a) Reflection of an incoming chirped pulse (blue) by a chirped plasma grating (position indicated by gray line), resulting in a strongly compressed reflected pulse (red line). Shown are the electric fields of the laser pulses normalized to the maximum of the incoming laser pulse. The plasma density n_e/n_c has been scaled by a factor 20 for better visibility. The incoming laser pulse has a maximum intensity of 10^{14} W/cm^2. (b) Energy spectrum $|E(k)|^2$ of incoming probe pulse (dashed line), reflected pulse (red line), and transmitted pulse (orange line).

find that the two curves in Fig. 6 show good agreement in terms of width and maximum amplitude. The analytic curve, however, predicts a steeper rise and fall of the reflectivity, respectively, in the wings. The PIC results show a more smooth, Gaussian-like profile. We attribute this to the fact that the actual grating has a smooth Gaussian envelope [indicated by the solid line in Fig. 1(a)], compared to the assumption of a constant amplitude grating in the analytic model. Nevertheless, the overall agreement between the two results is good.

V. SUMMARY AND OUTLOOK

The present work addresses the question of how a plasma-based grating can be generated and utilized for compressing previously amplified broad laser pulses. In addition to other proposals, the superposition of two chirped pump lasers is employed here, inducing density fluctuations in a plasma. Depending on the configuration of the pump lasers, either chirped or unchirped inhomogeneous grids are formed. Simple theoretical analysis demonstrates that ponderomotive forces are responsible for this phenomenon. The analytical considerations fully support the results of PIC simulations.

Following a thorough understanding of grid formation, the transmission and reflection behavior of individual spectral components (plane waves) is examined using a simple model. This involves the coupled mode equations, which can be analytically solved in the case of a homogeneous chirped grid. The assumption of homogeneity could be overcome by connecting individual layers in series and solving analytically for each layer. However, we refrain from this enhancement here, as we already know from previous work [33] the differences between homogeneous and Gaussian gratings.

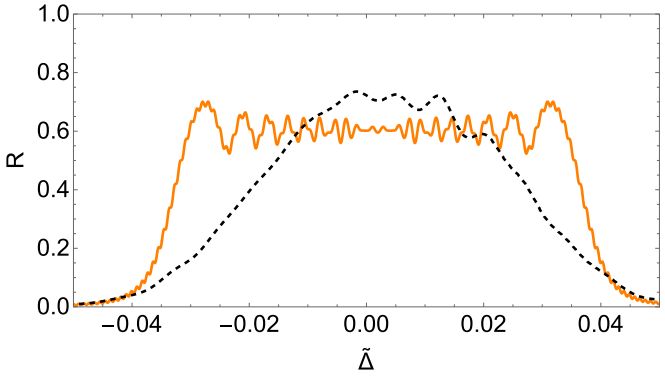

FIG. 6. Reflection coefficient R as obtained from (54) (orange solid line) for parameters resembling the chirped grating shown in Fig. 1(a). The black dashed line shows the reflection coefficient obtained from the PIC results shown in Fig. 5(b).

The analytical model calculations are particularly interesting because they allow for simple predictions regarding the behavior of the grid depending on various parameters such as chirp rate, amplitude, and length of the pump pulses. They apply to individual spectral components of an input pulse, and we can assume that their superposition fairly represents the pulse behavior. The latter is precisely demonstrated in the third part of the paper, where PIC simulations simulate the interaction of a chirped probe pulse with the chirped plasma-based grating. This allows for a very good estimation of the bandwidth.

For applications, central questions revolve around the lifetime and quality of the grating, as well as potential repetition and compression rates. We have only presented exemplary cases in this regard. A systematic investigation is still pending. We consider the present work as a proof of principle and hope for experimental realization. In this regard, we find ourselves in a constructive comparative situation with the plasma-based concept of a transmission grating for the compression of high-intensity laser pulses [7]. The latter currently seems to be somewhat closer to experimental realization. The theoretical evaluations presented here appear to show similarly favorable values as in Ref. [7]. However, as theoreticians, we should not speculate too much about the potential advantages or disadvantages of our plasma-based reflection grating concept but rather leave that evaluation to the experimental physicists.

ACKNOWLEDGMENTS

Computational support and infrastructure was provided by the Centre for Information and Media Technology (ZIM) at the University of Düsseldorf (Germany). Development of the EPOCH PIC code used in this work was in part funded by the

UK EPSRC Grants No. EP/G054950/1, No. EP/G056803/1, No. EP/G055165/1, and No. EP/M022463/1. We thank Mirela Cerchez for fruitful discussions on CPA gratings.

APPENDIX A: COUPLED MODE EQUATIONS FOR A GRATING WITH LINEAR CHIRP

The coupled mode system will be used to interpret the numerical PIC results. We first set up the basic equations. Subsequently we discuss appropriate boundary conditions to determine the transmission and reflection coefficient. As a byproduct of the general formulation, we can infer the influence of inhomogeneous density variations compared to the chirp effect. The investigation benefits from previous papers [14,15,36,48,49] on group delay in Bragg gratings with linear chirp.

Within a coupled mode analysis we start with incident plane waves. The individual waves can be interpreted as spectral contributions to pulses. Therefore, the reflections shown here are not directly applicable to the reflected pulses in PIC simulations. Nevertheless, they will be extremely helpful for interpreting the PIC results.

1. General form

We consider a plane test wave $E \sim e^{-i\omega t}$ with frequency ω such that (before normalization) the stationary amplitudes will be obtained from

$$\frac{d^2E}{dx^2} + k^2\frac{N^2}{N_0^2}E = 0 \tag{A1}$$

with

$$k \equiv \frac{\omega N_0}{c}, \quad N = \sqrt{1 - \frac{\omega_{pe}^2}{\omega^2}}. \tag{A2}$$

N is the refractive index, and N_0 is a reference index. Obviously, when the test wave frequency approaches the pump frequency, i.e., $\omega \to \omega_0$, we have

$$k \to k_1 \equiv \frac{\omega_0 N_0}{c}, \quad N \to N_0 = \sqrt{1 - \frac{\omega_{pe}^2}{\omega_0^2}}. \tag{A3}$$

From the (dimensional) wave number k_1 and the (dimensional) space-coordinate x we may construct the nondimensional variable

$$\xi = k_1 x = \frac{k_1}{k_0}\underbrace{k_0\lambda_0}_{2\pi}\frac{x}{\lambda_0} \hat{=} 2\pi N_0 x, \tag{A4}$$

where, in the last term on the r.h.s., x is dimensionless, i.e., normalized by λ_0. Normalization is performed using the following units. We normalize frequency ω by the pump frequency ω_0, time t by $2\pi/\omega_0$, distances with the laser wavelength λ_0 in vacuum, and wave numbers k by $k_0 \equiv \frac{2\pi}{\lambda_0}$. In plasma, the pump wave number is $k_1 = k_0 N_0$ with $N_0 = \sqrt{1 - n_0/n_c}$. The (constant) mean density n_0 will be used for density normalization, while the velocity of light c is the velocity unit. Then, $2k_1 x \to 4\pi N_0 x$ in nondimensional form. For the (normalized) frequency mismatch Δ we find

$$\Delta = \omega - 1 \quad \rightsquigarrow \quad k^2 \approx k_1^2(1 + 2\Delta) \tag{A5}$$

for $|\Delta| \ll 1$. Also

$$N^2 \approx N_0^2\left(1 + \left[1 - \frac{1}{N_0^2}\right]\delta n_e - \left[1 - \frac{1}{N_0^2}\right]2\Delta\right) \tag{A6}$$

and

$$k^2\frac{N^2}{N_0^2} \approx k_1^2\left(1 + \left[1 - \frac{1}{N_0^2}\right]\delta n_e + \frac{2}{N_0^2}\Delta\right). \tag{A7}$$

The electron density variation δn_e is driven by the ponderomotive force and (at least in the first part of the present discussion) may have an inhomogeneous contribution $\delta n_e^{inh} \sim D$. We write the ansatz in generalized form as

$$\delta n_e = \tfrac{1}{2}C(x)(e^{i\psi} + e^{-i\psi}) + D(x), \tag{A8}$$

where the coefficients C and D may still be space dependent. Furthermore,

$$\psi = 2\xi + \varphi(\xi). \tag{A9}$$

We allow for a (nonlinear) phase φ which becomes essential for chirped gratings. For example, linear chirp is equivalent to a quadratic phase

$$\varphi(\xi) = \beta(\xi - \xi_0)^2. \tag{A10}$$

The (normalized) wave equation (A1) takes the form

$$\frac{d^2E}{d\xi^2} + \left\{1 + \frac{2}{N_0^2}\Delta + \left[1 - \frac{1}{N_0^2}\right]D(\xi) + \frac{1}{2}\left[1 - \frac{1}{N_0^2}\right]C(\xi)\left(e^{2i\xi + i\varphi} + e^{-2i\xi - i\varphi}\right)\right\}E = 0. \tag{A11}$$

For the electric field E we make the ansatz

$$E(\xi) = a_+(\xi)e^{i\xi} + a_-(\xi)e^{-i\xi}, \tag{A12}$$

with slowly varying envelopes $a_\pm$. Later, we shall generalize to carrier wave numbers $k \neq k_1$. Within a slowly varying envelope approximation one obtains

$$\frac{da_+}{dx} = i\pi N_0\left[\frac{2}{N_0^2}\Delta + \left(1 - \frac{1}{N_0^2}\right)D\right]a_+ + i\frac{\pi N_0}{2}\left(1 - \frac{1}{N_0^2}\right)Ce^{i\varphi}a_-, \tag{A13}$$

$$\frac{da_-}{dx} = -i\pi N_0\left[\frac{2}{N_0^2}\Delta + \left(1 - \frac{1}{N_0^2}\right)D\right]a_- - i\frac{\pi N_0}{2}\left(1 - \frac{1}{N_0^2}\right)Ce^{-i\varphi}a_+. \tag{A14}$$

As mentioned already in several places, x is dimensionless (normalized by λ_0). For the amplitudes u and v, which are defined through

$$a_+(\xi) = u(\xi)e^{i\varphi/2}, \quad a_-(\xi) = v(\xi)e^{-i\varphi/2}, \tag{A15}$$

the standard coupled mode equations

$$\frac{du(\xi)}{d\xi} = i[\sigma(\xi)\,u(\xi) + \kappa(\xi)\,v(\xi)], \tag{A16}$$

$$\frac{dv(\xi)}{d\xi} = -i[\sigma(\xi)\,v(\xi) + \kappa(\xi)\,u(\xi)] \tag{A17}$$

appear. Here,

$$\sigma(\xi) = \frac{1}{N_0^2}\Delta + \frac{1}{2}\left(1 - \frac{1}{N_0^2}\right)D(\xi) - \frac{1}{2}\frac{d\varphi}{d\xi}, \quad \text{(A18)}$$

$$\kappa(\xi) = \frac{1}{4}\left(1 - \frac{1}{N_0^2}\right)C(\xi). \quad \text{(A19)}$$

2. Discussion of inhomogeneity versus chirp

Now we would like to point out an interesting general point. Equation (A18) shows that two terms occur side by side, namely a possible inhomogeneity in density and the derivative of the phase, i.e.,

$$\frac{1}{2}\left(1 - \frac{1}{N_0^2}\right)D(\xi) \hat{=} -\frac{1}{2}\frac{d\varphi}{d\xi}. \quad \text{(A20)}$$

From this, we can conclude that linear chirp and linear density variation are equivalent to each other.

Since plasma gratings are produced by pump pulses with nonconstant envelopes, the generation of a pure linear density grating might be difficult (or even impossible).

In applications, exponential variations might appear in addition, i.e.

$$D(\xi) \sim \exp\left(-\frac{\xi^2}{\xi_0^2}\right) \quad \text{(A21)}$$

might additionally occur. The latter then corresponds to a certain behavior of φ, namely

$$\varphi(\xi) \sim -\int^{\xi} D(\xi')d\xi' \sim \frac{\sqrt{\pi}}{2}\mathrm{erf}\left(\frac{\xi}{\xi_0}\right). \quad \text{(A22)}$$

Since the Taylor series of the error function is

$$\mathrm{erf}(x) \approx \frac{2}{\sqrt{\pi}}x - \frac{2}{3\sqrt{\pi}}x^3 + \mathcal{O}(x^5), \quad \text{(A23)}$$

we always expect from a Gaussian inhomogeneity a third-order phase contribution, which should be minimized. In other words, it will be challenging to produce a grating with a purely linear chirp. Corrections due to quadratic chirp can always be expected due to the inhomogeneous envelopes.

3. Boundary conditions

Now a few remarks concerning boundary conditions and the definition of reflection as well as transmission coefficients. Since in nondimensional form

$$2\pi N_0(1+\Delta)x = 2\pi kx, \quad \text{(A24)}$$

we may introduce

$$\sigma = \Delta - \frac{1}{2}\frac{d\varphi}{d\xi} + \bar{\sigma}, \quad \tilde{u} = u\,e^{-i\Delta\xi + i\varphi/2}, \quad \tilde{v} = v\,e^{i\Delta\xi - i\varphi/2}, \quad \text{(A25)}$$

to obtain the test electric field (in non-dimensional form) with appropriate carrier wave number k,

$$E = \tilde{u}(\xi)\,e^{2\pi ikx} + \tilde{v}(\xi)\,e^{-2\pi ikx}. \quad \text{(A26)}$$

The corresponding modified coupled mode equations are

$$\frac{d\tilde{u}(\xi)}{d\xi} = i[\bar{\sigma}(\xi)\,\tilde{u}(\xi) + \kappa(\xi)\,e^{-2i\Delta\xi + i\varphi}\,\tilde{v}(\xi)], \quad \text{(A27)}$$

$$\frac{d\tilde{v}(\xi)}{d\xi} = -i[\bar{\sigma}(\xi)\,\tilde{v}(\xi) + \kappa(\xi)\,e^{2i\Delta\xi - i\varphi}\,\tilde{u}(\xi)] \quad \text{(A28)}$$

with

$$\bar{\sigma}(\xi) = 2\pi N_0\left(1 - \frac{1}{N_0^2}\right)\left[\frac{1}{2}D(\xi) - \Delta\right]. \quad \text{(A29)}$$

When solving the coupled mode equations for a finite grating we remind the reader that ω_0 is the fixed frequency of the pumps creating the grating. The variable probe frequency is ω. Thus, with respect to the boundaries and the space variables, the transformation $\xi = 2\pi N_0 x$ is straightforward since for fixed n_0/n_c the factor N_0 will be constant.

For the region $-L \leqslant x \leqslant L$ we use the boundary conditions $\tilde{u}(x=-L) = 1$ and $\tilde{v}(x=L) = 0$. Then, the reflection coefficient R and the transmission coefficient T follow via

$$r = v(x=-L)e^{-i2\pi N_0\Delta L + i\varphi(x=-L)/2}$$

$$\rightarrow R \equiv |r|^2 = |v(x=-L)|^2, \quad \text{(A30)}$$

$$t = u(L)e^{-i2\pi N_0\Delta L + i\varphi(x=L)/2} \rightarrow T \equiv |t|^2 = |u(L)|^2. \quad \text{(A31)}$$

APPENDIX B: SOLUTION WITH HERMITE POLYNOMIALS

Here we present an alternative method for the solution of the basic equations (37) and (38). Solutions are the Hermite polynomials of imaginary order

$$U(\zeta) = H_{i/\chi_1}\left(\pm\sqrt{i\frac{\chi_1}{2}}\zeta\right), \quad V(\zeta) = H_{-i/\chi_1}\left(\pm\sqrt{i\frac{\chi_1}{2}}\zeta\right). \quad \text{(B1)}$$

They will be applied for $-L \leqslant x \leqslant L$, which translates into a region ζ between

$$\zeta_\pm = C_0 2\pi N_0(\pm L - x_0) - \frac{C_0}{\beta N_0^2}\Delta. \quad \text{(B2)}$$

As discussed before, the appropriate boundary conditions follow from $\tilde{u}(x=-L) = 1$ and $\tilde{v}(x=L) = 0$. We have to handle them for $U(\zeta)$ and $V(\zeta)$, having in mind the definition (34). Because of

$$\tilde{u}(\xi) = U(\zeta)e^{-i\left(1-\frac{1}{N_0^2}\right)\Delta\xi}, \quad \text{(B3)}$$

$$\tilde{v}(\xi) = V(\zeta)e^{i\left(1-\frac{1}{N_0^2}\right)\Delta\xi}, \quad \text{(B4)}$$

we obtain

$$U(\zeta_-) = e^{-i\left(1-\frac{1}{N_0^2}\right)\Delta 2\pi N_0 L}, \quad V(\zeta_+) = 0. \quad \text{(B5)}$$

When writing the general solution as

$$U(\zeta) = c_1\,H_{i/\chi_1}\left(\sqrt{i\frac{\chi_1}{2}}\zeta\right) + c_2\,H_{i/\chi_1}\left(-\sqrt{i\frac{\chi_1}{2}}\zeta\right), \quad \text{(B6)}$$

we may use (35) and (36) to obtain

$$V(\zeta) = \sqrt{\frac{2i}{\chi_1}}\left\{c_1 H_{i/\chi_1-1}\left(\sqrt{i\frac{\chi_1}{2}}\zeta\right) - c_2 H_{i/\chi_1-1}\left(-\sqrt{i\frac{\chi_1}{2}}\zeta\right)\right\}e^{2iZ}. \tag{B7}$$

The boundary conditions (B5) lead to an inhomogeneous linear system of equations for the coefficients c_1 and c_2 which has to be solved to obtain the complete analytic solution. We get

$$c_2 = \underbrace{\frac{H_{i/\chi_1-1}\left(\sqrt{i\frac{\chi_1}{2}}\zeta_+\right)}{H_{i/\chi_1-1}\left(-\sqrt{i\frac{\chi_1}{2}}\zeta_+\right)}}_{c_{211}} c_1 \equiv c_{211}c_1, \tag{B8}$$

$$c_1 = \frac{e^{-i\left(1-\frac{1}{N_0^2}\right)\Delta 2\pi N_0 L}}{H_{i/\chi_1}\left(\sqrt{i\frac{\chi_1}{2}}\zeta_-\right)} - c_{211}\, c_1 \underbrace{\frac{H_{i/\chi_1}\left(-\sqrt{i\frac{\chi_1}{2}}\zeta_-\right)}{H_{i/\chi_1}\left(\sqrt{i\frac{\chi_1}{2}}\zeta_-\right)}}_{c_{212}}, \tag{B9}$$

or

$$c_1 = \frac{1}{1+c_{211}\,c_{212}}\,\frac{e^{-i\left(1-\frac{1}{N_0^2}\right)\Delta 2\pi N_0 L}}{H_{i/\chi_1}\left(\sqrt{i\frac{\chi_1}{2}}\zeta_-\right)}. \tag{B10}$$

Having determined the coefficients c_1 and c_2 we may determine the transmission coefficient T as well as the reflection coefficient R from (B6). The result is

$$T = |\tilde{u}(x=+L)|^2 = |U(\zeta_+)|^2, \tag{B11}$$

$$R = |\tilde{v}(x=-L)|^2 = |V(\zeta_-)|^2. \tag{B12}$$

The formulas prompt two remarks. First, we may estimate the extent to which the chirp alters the effectiveness of the grating in reflection compared to an unchirped grid. Furthermore, examining the argument in the Hermite polynomials is insightful. It demonstrates a variation with the chirp parameter of the grating. Consequently, an incident plane wave is reflected with a slight change in effective wavelength.

[1] D. Strickland and G. Mourou, Compression of amplified chirped optical pulses, Opt. Commun. **55**, 447 (1985).

[2] G. A. Mourou, C. P. J. Barry, and M. D. Perry, Ultrahigh-intensity lasers: Physics on the extreme on a tabletop, Phys. Today **51**(1), 22 (1998).

[3] L. Glebov, V. Smirnov, E. Rotari, I. Cohanoschi, L. Glebova, O. Smolski, J. Lumeau, C. Lantigua, and A. Glebov, Volume-chirped Bragg gratings: Monolithic components for stretching and compression of ultrashort laser pulses, Opt. Eng. **53**, 051514 (2014).

[4] H. Peng, J.-R. Marquès, L. Lancia, F. Amiranoff, R. L. Berger, S. Weber, and C. Riconda, Plasma optics in the context of high intensity lasers, Matter Radiat. Extremes **4**, 065401 (2019).

[5] Y. Michine and H. Yoneda, Ultra high damage threshold optics for high power lasers, Commun. Phys. **3**, 24 (2020).

[6] P. Michel, Plasma photonics: Manipulating light using plasmas, Lawrence Livermore National Laboratory technical report, 2021 (unpublished).

[7] M. R. Edwards and P. Michel, Plasma transmission gratings for compression of high-intensity laser pulses, Phys. Rev. Appl. **18**, 024026 (2022).

[8] J. Dutta Majumdar and I. Manna, Laser material processing, Int. Mater. Rev. **56**, 341 (2011).

[9] V. Malka, J. Faure, Y. A. Gauduel, E. Lefebvre, A. Rousse, and K. T. Phuoc, Principles and applications of compact laser-plasma accelerators, Nat. Phys. **4**, 447 (2008).

[10] Q. Peng, A. Juzeniene, J. Chen, L. Svaasand, T. Warloe, K.-E. Giercksky, and J. Moan, Lasers in medicine, Rep. Prog. Phys. **71**, 056701 (2008).

[11] F. Krausz and M. Ivanov, Attosecond physics, Rev. Mod. Phys. **81**, 163 (2009).

[12] H. Abu-Shawareb *et al.* (Indirect Drive ICF Collaboration), Lawson criterion for ignition exceeded in an inertial fusion experiment, Phys. Rev. Lett. **129**, 075001 (2022).

[13] Z.-M. Sheng, J. Zhang, and D. Umstadter, Plasma density gratings induced by intersecting laser pulses in underdense plasmas, Appl. Phys. B **77**, 673 (2003).

[14] H.-C. Wu, Z.-M. Sheng, Q.-J. Zhang, Y. Cang, and J. Zhang, Controlling ultrashort intense laser pulses by plasma Bragg gratings with ultrahigh damage threshold, Laser Part. Beams **23**, 417 (2005).

[15] H.-C. Wu, Z.-M. Sheng, Q.-J. Zhang, Y. Cang, and J. Zhang, Manipulating ultrashort intense laser pulses by plasma Bragg gratings, Phys. Plasmas **12**, 113103 (2005).

[16] H.-C. Wu, Z.-M. Sheng, and J. Zhang, Chirped pulse compression in nonuniform plasma Bragg gratings, Appl. Phys. Lett. **87**, 201502 (2005).

[17] S. Suntsov, D. Abdollahpour, D. G. Papazoglou, and S. Tzortzakis, Femtosecond laser induced plasma diffraction gratings in air as photonic devices for high intensity laser applications, Appl. Phys. Lett. **94**, 251104 (2009).

[18] M. Durand, Y. Liu, B. Forestier, A. Houard, and A. Mysyrowicz, Experimental observation of a traveling plasma grating formed by two crossing filaments in gases, Appl. Phys. Lett. **98**, 121110 (2011).

[19] S. Monchocé, S. Kahaly, A. Leblanc, L. Videau, P. Combis, F. Réau, D. Garzella, P. D'Oliveira, P. Martin, and F. Quéré, Optically controlled solid-density transient plasma gratings, Phys. Rev. Lett. **112**, 145008 (2014).

[20] L.-L. Yu, Y. Zhao, L.-J. Qian, M. Chen, S.-M. Weng, Z.-M. Sheng, D. A. Jaroszynski, W. B. Mori, and J. Zhang, Plasma optical modulators for intense lasers, Nat. Commun. **7**, 11839 (2016).

[21] G. Lehmann and K. H. Spatschek, Transient plasma photonic crystal for high-power lasers, Phys. Rev. Lett. **116**, 225002 (2016).

[22] G. Lehmann and K. H. Spatschek, Laser-driven plasma photonic crystals for high-power lasers, Phys. Plasmas **24**, 056701 (2017).

[23] G. Lehmann and K. H. Spatschek, Plasma photonic crystal growth in the trapping regime, Phys. Plasmas **26**, 013106 (2019).
[24] H. Peng, C. Riconda, M. Grech, J.-Q. Su, and S. Weber, Nonlinear dynamics of laser-generated ion-plasma gratings: A unified description, Phys. Rev. E **100**, 061201(R) (2019).
[25] H. Peng, C. Riconda, M. Grech, C.-T. Zhou, and S. Weber, Dynamical aspects of plasma gratings driven by a static ponderomotive potential, Plasma Phys. Controlled Fusion **62**, 115015 (2020).
[26] H. H. Ma, S. M. Weng, P. Li, Y. X. Wang, S. H. Yew, M. Chen, P. M. McKenna, and Z. M. Sheng, Growth, saturation, and collapse of laser-driven plasma density gratings, Phys. Plasmas **27**, 073105 (2020).
[27] C. Zhang, Z. Nie, Y. Wu, M. Sinclair, C.-K. Huang, K. A. Marsh, and J. Chan, Ionization induced plasma grating and its applications in strong-field ionization measurements, Plasma Phys. Controlled Fusion **63**, 095011 (2021).
[28] G. Lehmann and K. H. Spatschek, Reflection and transmission properties of a finite-length electron plasma grating, Matter Radiat. Extremes **7**, 054402 (2022).
[29] G. Vieux, S. Cipiccia, G. H. Welsh, S. R. Yoffe, F. Gartner, M. P. Tooley, B. Ersfeld, E. Brunetti, B. Eliasson, C. Picken, G. McKendrick, M. S. Hur, J. M. Dias, T. Kuehl, G. Lehmann, and D. A. Jaroszynski, The role of transient plasma photonic structures in plasma-based amplifiers, Commun. Phys. **6**, 9 (2023).
[30] Y. X. Wang, X. L. Zhu, S. M. Weng, P. Li, X. F. Li, H. Ai, H. R. Pan, and Z. M. Sheng, Fast efficient photon deceleration in plasmas by using two laser pulses at different frequencies, Matter Radiat. Extremes **9**, 037201 (2024).
[31] J. E. Sipe, L. Poladian, and C. M. de Sterke, Propagation through nonuniform grating structures, J. Opt. Soc. Am. A **11**, 1307 (1994).
[32] L. Poladian, Graphical and WKB analysis of nonuniform Bragg gratings, Phys. Rev. E **48**, 4758 (1993).
[33] G. Lehmann and K.-H. Spatschek, Formation and properties of spatially inhomogeneous plasma density gratings, Phys. Rev. E **108**, 055204 (2023).
[34] R. Szipöcs, K. Ferencz, C. Spielmannn, and F. Krausz, Chirped multilayer coatings for broadband dispersion control in femtosecond lasers, Opt. Lett. **19**, 201 (1994).
[35] M. Sumetsky, B. J. Eggleton, and C. M. deSterke, Theory of group delay ripple generated by chirped fiber gratings, Opt. Express **10**, 332 (2002).
[36] O.V. Belai, E.V. Podivilov, and D. A. Shapiro, Group delay in Bragg grating with linear chirp, Opt. Commun. **266**, 512 (2006).
[37] S. Kaim, S. Mokhov, B.Y. Zeldovich, and L. B. Glebov, Stretching and compressing of short laser pulses by chirped Bragg gratings: Analytic and numerical modeling, Opt. Eng. **53**, 051509 (2014).
[38] Z. Rongrong and C. Ping, Analysis on the reflection characteristic and the dispersion compensation performance of linear chirped fiber grating, Inf. Technol. J. **13**, 1868 (2014).
[39] Z. Tian and L. Yu, Rainbow trapping of ultrasonic guided waves in chirped phononic crystal plates, Sci. Rep. **7**, 1 (2017).
[40] I. Ulyanov, Theoretical analysis of the stretched optical pulse ripple and novel chirped pulse retrieving algorithm, Opt. Express **27**, 28166 (2019).
[41] M. S. Hur, B. Ersfeld, H. Lee, H. Kim, K. Roh, Y. Lee, H. S. Song, M. Kumar, S. Yoffe, D. A. Jaroszynski, and H. Suk, Laser pulse compression by a density gradient plasma for exawatt to zettawatt lasers, Nat. Photon. **17**, 1074 (2023).
[42] H. Kogelnik, Coupled wave theory for thick hologram gratings, Bell Syst. Tech. J. **48**, 2909 (1969).
[43] M. R. Rernandez-Ruiz and A. Carballar, Fiber Bragg grating-based optical signal processing: Review and survey, Appl. Sci. **11**, 8189 (2021).
[44] T. D. Arber, K. Bennett, C. S. Brady, A. Lawrence-Douglas, M. G. Ramsay, N. J. Sircombe, P. Gillies, R. G. Evans, H. Schmitz, A. R. Bell, and C. P. Ridgers, Contemporary particle-in-cell approach to laser-plasma modelling, Plasma Phys. Controlled Fusion **57**, 113001 (2015).
[45] L. Roso, High repetition rate petawatt lasers, EPJ Web Conf. **167**, 01001 (2018).
[46] D. A. Alessi, P. A. Rosso, H. T. Nguyen, M. D. Aasen, J. A. Britten, and C. Haefner, Active cooling of pulse compression diffraction gratings for high energy, high average power ultrafast lasers, Opt. Express **24**, 30015 (2016).
[47] V. Leroux, T. Eichner, and A. R. Maier, Description of spatio-temporal couplings from heat-induced compressor grating deformation, Opt. Express **28**, 8257 (2020).
[48] Z. Wu, Q. Chen, A. Morozov, and S. Suckewer, Compression of laser pulses by near-forward Raman amplification in plasma, Phys. Plasmas **27**, 013104 (2020).
[49] Z. Wu, Y. Zuo, X. Zeng, Z. Li, Z. Zhang, X. Wang, B. Hu, X. Wang, J. Mu, J. Su, Q. Zhu, and Y. Dai, Laser compression via fast-extending plasma gratings, Matter Radiat. Extremes **7**, 064402 (2022).